Eur. Phys. J. E **5**, 161–170 (2001)

THE EUROPEAN PHYSICAL JOURNAL E

EDP Sciences

Heated granular fluids: The random restitution coefficient approach

A. Barrat[1,a], E. Trizac[1], and J.-N. Fuchs[2]

[1] Laboratoire de Physique Théorique[b], Bâtiment 210, Université de Paris-Sud, 91405 Orsay, France
[2] Laboratoire Kastler-Brossel[c], Département de Physique de l'E.N.S, 24 rue Lhomond, 75231 Paris, France

Received 24 November 2000 and Received in final form 8 February 2001

Abstract. We introduce the model of inelastic hard spheres with random restitution coefficient α, in order to account for the fact that, in a vertically shaken granular system interacting elastically with the vibrating boundary, the energy injected vertically is transferred to the horizontal degrees of freedom through collisions only, which leads to heating through collisions, *i.e.* to inelastic horizontal collisions with an effective restitution coefficient that can be larger than 1. This allows the system to reach a non-equilibrium steady state, where we focus, in particular, on the single-particle velocity distribution $f(v)$ in the horizontal plane, and on its deviation from a Maxwellian. Molecular Dynamics simulations and Direct Simulation Monte Carlo (DSMC) show that, depending on the distribution of α, different shapes of $f(v)$ can be obtained, with very different high-energy tails. Moreover, the fourth cumulant of the velocity distribution quantifying the deviations from Gaussian statistics is obtained analytically from the Boltzmann equation and successfully tested against the simulations.

PACS. 45.70.-n Granular systems – 51.10.+y Kinetic and transport theory of gases – 45.10.-b Computational methods in classical mechanics

1 Introduction

Despite a wealth of recent experimental investigations, it seems that there is no consensus yet as to the characteristics of the collective behaviour of vibrated granular mono- or multi-layers [1–6]. Among the statistical properties of interest, the velocity fluctuations and, more precisely, the deviations from Maxwell-Boltzmann distribution due to inelastic collisions have been intensively studied for rapid granular flows, and several groups reported an overpopulated high-energy tail that can be fitted by stretched exponentials with various exponents.

Theoretical investigations commonly use the inelastic hard spheres (IHS) model [7,8], which has proven very useful despite the simplicity of its definition: smooth hard spheres undergo binary inelastic momentum-conserving collisions, thereby losing during the collision a constant fraction of their relative normal velocity (and therefore losing energy). Many studies have concentrated on the homogeneous cooling state of the IHS [9–14], obtained by letting the system evolve without any energy injection. On the other hand, experiments on strongly vibrated granular media consider systems that are heated by an external forcing (*e.g.*, a vertically oscillating plate) to compensate for the energy loss due to collisions, and are therefore in a non-equilibrium stationary state (NESS). Various ways of modeling the heating mechanism have been put forward, mostly consisting in the study of an effective system with a constant coefficient of normal restitution α, in which the energy lost through collisions is balanced by energy injected by random "kicks" [15–19]. In this context, analytical and numerical results have been obtained for the high-energy tail of the velocity distributions and for its fourth cumulant, a natural measure of the deviation from a Gaussian distribution [12,17,20]. Moreover, more realistic Molecular Dynamics simulations of vibrated soft-sphere mono-layers [21] have been able to reproduce the phenomenology obtained in some experiments [3].

In this paper, we propose an alternative modeling of a three-dimensional system shaken vertically along the z-axis, for which the velocities are studied both numerically and analytically in the horizontal (x, y)-plane. If the collisions with the boundaries are elastic, the vibrating wall feeds energy in the system in the z-direction only, but not in the (x, y)-plane where the corresponding two-dimensional energy is either lost or gained at each collision between two grains. Upon restricting to the xy velocities, we obtain a system that is subject to an effective stationary dynamics with sequential energy injection or dissipation consecutive to particle-particle collisions only.

[a] e-mail: `Alain.Barrat@th.u-psud.fr`
[b] Unité Mixte de Recherche UMR 8627
[c] Unité Mixte de Recherche UMR 8552

We shall thus disregard the vibrating boundary and concentrate on the effective planar dynamics where energy gains and losses statistically cancel in the NESS, so that an effective restitution coefficient can either be larger or smaller than 1; this will be accounted for by a *random* α, drawn from a probability distribution $\rho(\alpha)$ (such that the second moment $\overline{\alpha^2} = 1$ in order to conserve energy on average). Our approach, in which momentum transfer occurs only through collisions, consequently differs from the situations investigated in [15–19] where energy is injected globally into the system at regular time intervals through a stochastic external force. Clearly, the functional form of $\rho(\alpha)$ reflects the energy injection mechanism, and it is a difficult task to establish this connection. The physical situations that could be described by the present model are mono- or multi-layers of grains provided the interactions with the wall are elastic, or a multilayer system with arbitrary interactions with the wall, in a "bulk" region far from the boundaries where energy and density can be considered as constant. In a very different context, a similar stochastic coefficient of restitution has been introduced to study the dynamics of a one-dimensional granular gas, thereby accounting for internal degrees of freedom [22].

The paper is organized as follows: after setting the general framework in Section 2, we consider the two-dimensional projection of three-dimensional simulations of inelastic hard spheres with constant restitution coefficient α, energy being injected in the third direction (Sect. 3). We analyze, in particular, the distribution of energy transfer through collisions. In Section 4, the two-dimensional IHS model with random restitution coefficient is then studied by analytical and numerical means. Section 5 is devoted to a short investigation of the one-dimensional case, and some conclusions are finally presented in Section 6.

2 General framework

2.1 IHS: definitions and notations

In the inelastic hard spheres (IHS) model, grains are modeled as smooth hard spheres of mass m undergoing binary, inelastic and momentum-conserving collisions: a collision between two spheres labeled by 1 and 2, with velocities $\mathbf{v}_1$ and $\mathbf{v}_2$, dissipates a fraction $(1-\alpha)$ of the component of the relative velocity $\mathbf{v}_{12} = \mathbf{v}_1 - \mathbf{v}_2$ along the center-to-center direction $\hat{\boldsymbol{\sigma}}$. Noting with stars the post-collision velocities, this translates into $\mathbf{v}_{12}^* \cdot \hat{\boldsymbol{\sigma}} = -\alpha\, \mathbf{v}_{12} \cdot \hat{\boldsymbol{\sigma}}$, while the tangential relative velocity (perpendicular to $\hat{\boldsymbol{\sigma}}$) is conserved, *i.e.*

$$\mathbf{v}_1^* = \mathbf{v}_1 - \frac{1}{2}(1+\alpha)(\mathbf{v}_{12}\cdot\hat{\boldsymbol{\sigma}})\hat{\boldsymbol{\sigma}}\,,$$
$$\mathbf{v}_2^* = \mathbf{v}_2 + \frac{1}{2}(1+\alpha)(\mathbf{v}_{12}\cdot\hat{\boldsymbol{\sigma}})\hat{\boldsymbol{\sigma}}\,. \tag{1}$$

These equations are also sometimes written in terms of restituting collisions, *i.e.* for collisions which yield $(\mathbf{v}_1, \mathbf{v}_2)$ as post-collisional velocities, for pre-collisional velocities $(\mathbf{v}_1^{**}, \mathbf{v}_2^{**})$:

$$\mathbf{v}_1^{**} = \mathbf{v}_1 - \frac{1}{2}\left(1+\frac{1}{\alpha}\right)(\mathbf{v}_{12}\cdot\hat{\boldsymbol{\sigma}})\hat{\boldsymbol{\sigma}}\,,$$
$$\mathbf{v}_2^{**} = \mathbf{v}_2 + \frac{1}{2}\left(1+\frac{1}{\alpha}\right)(\mathbf{v}_{12}\cdot\hat{\boldsymbol{\sigma}})\hat{\boldsymbol{\sigma}}\,. \tag{2}$$

2.2 Evolution equation

The Enskog-Boltzmann equation describes the evolution of the one-particle distribution function $f(\mathbf{r}, \mathbf{v}, t)$, upon the molecular chaos hypothesis [23]. In the homogeneous case, for hard spheres of diameter σ, in d dimensions, this equation reads

$$\frac{\partial f(\mathbf{v}_1,t)}{\partial t} = \chi\sigma^{d-1}\int \mathrm{d}\mathbf{v}_2 \int' \mathrm{d}\hat{\boldsymbol{\sigma}}(\mathbf{v}_{12}\cdot\hat{\boldsymbol{\sigma}}) \times\left\{\frac{1}{\alpha^2} f(\mathbf{v}_1^{**},t) f(\mathbf{v}_2^{**},t) - f(\mathbf{v}_1,t) f(\mathbf{v}_2,t)\right\} \equiv \chi I(f,f)\,. \tag{3}$$

The prime on the integration symbol is a shortcut for $\int \mathrm{d}\hat{\boldsymbol{\sigma}}\Theta(\mathbf{v}_{12}\cdot\hat{\boldsymbol{\sigma}})$, where Θ is the Heavyside function, while χ accounts for excluded-volume effects (for elastic hard spheres, χ coincides with the density-dependent pair correlation function at contact). The forcing mechanism necessary to sustain a NESS can be of different types, and has not been introduced in equation (3). This issue will be addressed in Section 4.

2.3 Sonine expansion for the velocity distribution

Because of analytical, numerical and experimental evidences, it is customary to look for scaling solutions of equation (3), in the form [24]

$$f(\mathbf{v},t) = \frac{n}{v_0^d(t)}\tilde{f}\left(\frac{v}{v_0(t)}\right)\,, \tag{4}$$

where n is the density and the thermal velocity v_0 is by definition related to the temperature $T(t)$ through $\frac{m}{2}v_0^2(t) = T(t)$, where in turn the temperature is defined by the average kinetic energy of the particles:

$$\frac{dn}{2}T(t) = \int \mathrm{d}\mathbf{v}\frac{m}{2}v^2 f(\mathbf{v},t)\,. \tag{5}$$

Replacing the scaling function in equation (3), together with the law of evolution of the temperature (see [17] for details) yields the following equation:

$$\frac{\mu_2}{d}\left(d + c_1\frac{\mathrm{d}}{\mathrm{d}c_1}\right)\tilde{f}(c_1) = \tilde{I}(\tilde{f},\tilde{f})\,, \tag{6}$$

where $\mathbf{c}_i = \mathbf{v}_i/v_0(t)$,

$$\tilde{I}(\tilde{f},\tilde{f}) = \int \mathrm{d}\mathbf{c}_2 \int' \mathrm{d}\hat{\boldsymbol{\sigma}}(\mathbf{c}_{12}\cdot\hat{\boldsymbol{\sigma}}) \times\left\{\frac{1}{\alpha^2}\tilde{f}(c_1^{**})\tilde{f}(c_2^{**}) - \tilde{f}(c_1)\tilde{f}(c_2)\right\}\,, \tag{7}$$

and $\mu_p \equiv -\int \mathrm{d}\mathbf{c}_1 c_1^p \tilde{I}(\tilde{f},\tilde{f})$.

In the elastic case ($\alpha = 1$), $\tilde{f}$ is the Gaussian $\Phi(c) = \pi^{-d/2}\exp(-c^2)$ (since $\tilde{I}(\Phi,\Phi) = 0$). The deviations from Φ are studied by an expansion in terms of Sonine polynomials [25]

$$\tilde{f}(c) = \Phi(c)\left(1 + \sum_{p=1}^{\infty} a_p S_p(c^2)\right) . \tag{8}$$

Indeed, the coefficients a_p can be obtained from the moments of $\tilde{f}$, because the S_p satisfy the orthogonality relations

$$\int \mathrm{d}\mathbf{c}\Phi(c) S_p(c^2) S_{p'}(c^2) = \delta_{pp'} N_p \,, \tag{9}$$

where the N_p are normalization constants. These polynomials consequently depend on the dimension d; the first ones read

$$\begin{aligned} S_0(x) &= 1 \,, \\ S_1(x) &= -x + \frac{d}{2} \,, \\ S_2(x) &= \frac{x^2}{2} - \frac{d+2}{2}x + \frac{d(d+2)}{8} \,. \end{aligned} \tag{10}$$

The orthogonality properties allow to write

$$a_p = \frac{1}{N_p}\langle S_p(c^2)\rangle. \tag{11}$$

In particular, $a_1 = (2/d)(-\langle c^2\rangle + d/2)$ vanishes because of the definition of temperature, and a_2 is related to the fourth cumulant of $\tilde{f}$:

$$a_2 = \frac{4\langle c^4\rangle}{d(d+2)} - 1 \,. \tag{12}$$

In Section 4, we shall briefly recall the different steps involved in the computation of a_2 that quantifies the deviations from Gaussianity.

2.4 DSMC method

The Direct Simulation Monte Carlo (DSMC) method allows to solve numerically the Boltzmann equation (3) [26]. It has been successfully used, *e.g.*, for the study of the homogeneous cooling state of the IHS, in [11] to assess the validity of the Sonine expansion, and in [27] to analyze the high-energy tail of $\tilde{f}$. In [20], the case of heated granular fluids has also been considered and compared to the theoretical predictions of [17].

The positions of the particles do not appear in equation (3). Therefore, all reference to space is here useless; this amounts, in the usual DSMC language, to taking only one cell where all particles stand, and of course eliminates the possibility to study spatial inhomogeneities. Moreover, upon an appropriate rescaling of time, we shall take $\chi = 1$ and $\sigma = 1$. Since no external force is present, the velocities of the particles do not change between collisions, and no "free streaming stage" is here necessary, and the simulation has the following scheme: we start from N particles with random velocities taken from an arbitrary distribution (*e.g.*, Gaussian, or flat); then the evolution proceeds by choosing at random pairs of particles (i,j), a direction $\hat{\boldsymbol{\sigma}}$ for their center-to-center direction, and updating their velocities according to the collision rule with a probability proportional to $\Theta(\mathbf{v}_{ij}\cdot\hat{\boldsymbol{\sigma}})\mathbf{v}_{ij}\cdot\hat{\boldsymbol{\sigma}}$. Once a stationary state is reached, running averages can be taken on the quantities of interest.

2.5 Molecular Dynamics simulations

The Molecular Dynamics (MD) simulations integrate the exact equation of motion of the model, with no reference to the Boltzmann equation: we consider N spheres of diameter σ, in a box of linear size L in dimension d, with periodic boundary conditions [28,29]. These spheres initially have random velocities, and we use an event-driven algorithm to study their dynamics. Once more, running averages are taken once a stationary state is reached.

3 2D projection of a 3D system

We consider an IHS model with constant (velocity-independent) restitution coefficient $\alpha < 1$, in dimension $d = 3$, the Cartesian coordinates being labeled x, y and z. The collisions are dissipative but energy is re-injected in the vertical direction (z) in the following way: after each collision, the z-component of the velocity of the particles having collided is randomly drawn from a Gaussian distribution at fixed temperature, while the x-y components remain those resulting from the initial inelastic collision. This procedure is intended to mimic both the energy injection due to a vibrating wall, and transfer to horizontal degrees of freedom through collisions only: indeed, a vibrating boundary can yield in the bulk of a multi-layer system an equilibrated Gaussian vertical velocity [2,30]. We could have used different vertical velocity distributions, in particular asymmetric ones, with the same conclusion: the point here is to illustrate the horizontal energy transfer mechanism.

Let us indeed analyze the system in the horizontal plane (x,y). After a transient, the two-dimensional temperature $T_{xy} = \frac{1}{2}(\langle v_x^2 + v_y^2\rangle)$ remains stationary (see the inset of Fig. 1): overall, *i.e.* when the three components of the velocities are considered, a collision is dissipative, but in the (x,y)-plane, energy can be gained by a transfer from the z-direction. In the horizontal plane, both phenomena compensate each other, as appears in Figure 1: the histogram of the energy transferred in the (x,y)-plane at each collision (given by $\Delta E = v_{1x}'^2 + v_{1y}'^2 + v_{2x}'^2 + v_{2y}'^2 - (v_{1x}^2 + v_{1y}^2 + v_{2x}^2 + v_{2y}^2)$, where 1 and 2 label the two colliding particles) has of course a negative part but also a positive one, corresponding to an energy gain in the (x,y)-plane

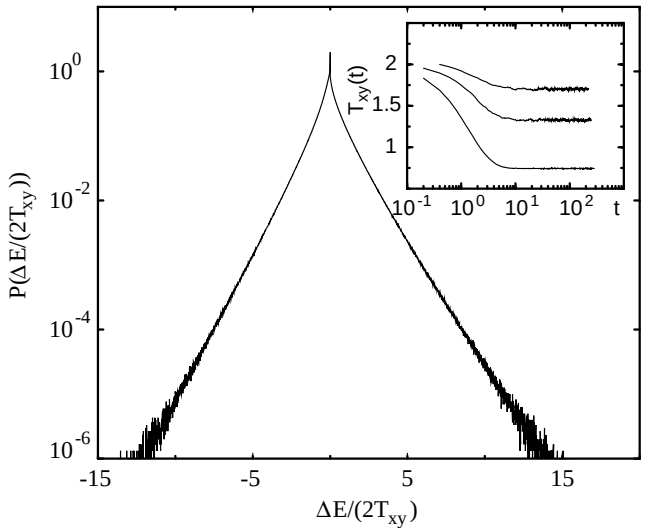

Fig. 1. Histogram of the two-dimensional energy change consecutive to a collision for a 3D DSMC simulation of a system of $N = 5 \cdot 10^5$ particles, with constant restitution coefficient $\alpha = 0.9$ and energy injection in the z-direction. The positive part corresponds to effective restitution coefficients larger than 1. The inset shows the transient approach to the NESS of the two-dimensional temperature for $\alpha = 1,\ 0.9,\ 0.6$ (from top to bottom). The initial value of the temperature coincides with that of the equilibrated vertical degrees of freedom. A similar anisotropy between horizontal and vertical temperatures has been observed in [21].

through a three-dimensional collision (the positive part would be absent in a simulation without heating and constant $\alpha < 1$). This positive part compensates the energy loss and allows to reach a NESS with a constant T_{xy}.

It would be feasible to inject energy in a more refined way, by considering, for instance, the collisions with the vibrating wall. Seeking for analytical results concerning the 2D horizontal velocity distribution, we shall however make the simplifying assumption that the effective 2D restitution coefficient decouples from the impact relative velocity. The resulting zeroth-order modeling introduced below displays qualitatively the same energy transfer behaviour as the projected 3D system and is amenable to a kinetic theory description.

4 Random restitution coefficient

We shall hereafter consider an IHS model for which, at each collision, the restitution coefficient is drawn from a probability distribution $\rho(\alpha)$. The means over $\rho(\alpha)$ will be denoted by an overline, and the distribution of α^2 by $\tilde{\rho}(\alpha^2)$. Since, in a binary collision with restitution coefficient α, the energy change is

$$\Delta E = \frac{m}{2}(\mathbf{v}_{12}^{**} \cdot \hat{\boldsymbol{\sigma}})^2 \frac{(\alpha^2 - 1)}{2} \tag{13}$$

(where $\mathbf{v}_{12}^{**}$ is the relative velocity before collision, $\hat{\boldsymbol{\sigma}}$ the center-to-center direction, and m the mass of the particles) and since the value of α is taken uncorrelated with the velocities of the particles, we shall consider distributions with $\overline{\alpha^2} = 1$ in order to ensure a stationary, constant-temperature regime (at each collision, energy changes, but is conserved on average: $\overline{\Delta E} = 0$). Moreover, we will restrict ourselves to positive values of α. Since the average energy is constant, the granular temperature is also a constant determined by the initial velocity distribution. This model is therefore intended to study the distribution of *rescaled* velocities $\mathbf{c} = \mathbf{v}/v_0$.

4.1 Analytical results

The methods of [17] for the case of constant normal restitution (with or without external heating) can be easily applied to the case of random α to systematically obtain the coefficients of the Sonine expansion. We refer to [17] for details and sketch only the principal steps. Note that the calculation is made under the hypothesis of a small a_2: the Sonine expansion (8) is therefore truncated after second order and besides, terms of order a_2^2 are discarded (it is possible to go beyond the linear approximation in a_2, with again truncation of (8) after $n = 2$; it was however shown that in the case of constant α, the correction is less than 10% [13]).

Once the moments $\mu_p \equiv -\int \mathrm{d}\mathbf{c}_1 c_1^p \tilde{I}(\tilde{f}, \tilde{f})$ have been defined, multiplying equation (6) by c_1^p and integrating over c_1 yields

$$\mu_p = \mu_2 \frac{p}{d} \langle c^p \rangle. \tag{14}$$

Taking $p = 4$ and approximating $\tilde{f}$ by its second-order Sonine expansion, it is now possible to evaluate μ_2, μ_4 and $\langle c^4 \rangle$, that can be averaged over α:

$$\begin{aligned} \langle c^4 \rangle &= \frac{d(d+2)}{4}(1 + a_2)\,, \\ \overline{\mu_2} &= \frac{\Omega_d}{2\sqrt{2\pi}}(1 - \overline{\alpha^2}) \left(1 + \frac{3}{16} a_2\right)\,, \\ \overline{\mu_4} &= \sqrt{\frac{2}{\pi}} \Omega_d (\overline{T_1} + a_2 \overline{T_2})\,, \end{aligned} \tag{15}$$

with $T_1 = (1-\alpha^2)(d+3/2+\alpha^2)/4$, $T_2 = 3(1-\alpha^2)(10d + 39 + 10\alpha^2)/128 + (1+\alpha)(d-1)/4$ (Ω_d is the volume of the d-dimensional unit sphere). Inserting these relations in (14) and neglecting terms of order a_2^2 leads to the final expression for a_2 in dimension d:

$$a_2 = 16 \frac{1 - 3\overline{\alpha^2} + 2\overline{\alpha^4}}{9 + 24d + 32(d-1)\overline{\alpha} + (8d-11)\overline{\alpha^2} - 30\overline{\alpha^4}}\,. \tag{16}$$

It can be checked that the expression obtained in [17] is recovered in the case of constant α: when $\rho(\alpha) = \delta(\alpha - \alpha_\star)$, we get

$$a_2 = 16 \frac{1 - \alpha_\star - 2\alpha_\star^2 + 2\alpha_\star^3}{9 + 24d + 8\alpha_\star d - 41\alpha_\star + 30(1-\alpha_\star)\alpha_\star^2}\,. \tag{17}$$

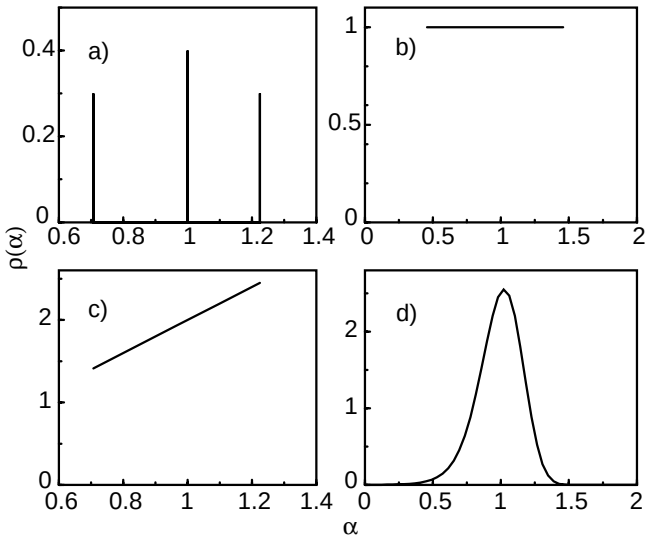

Fig. 2. Various distributions $\rho(\alpha)$ of the restitution parameter, fulfilling $\overline{\alpha^2} = 1$: a) trimodal distribution $\rho(\alpha) = \frac{b}{2}[\delta(\alpha - \sqrt{1+\gamma}) + \delta(\alpha - \sqrt{1-\gamma})] + (1-b)\delta(\alpha - 1)$, with the bimodal case included for $b = 1$; b) flat $\rho(\alpha)$ ($\alpha \in [0.457427; 1.457427]$); c) flat $\tilde{\rho}(\alpha^2)$ (*i.e.* linear $\rho(\alpha)$), for $\alpha^2 \in [1-\gamma, 1+\gamma]$; d) Gaussian $\tilde{\rho}(\alpha^2)$.

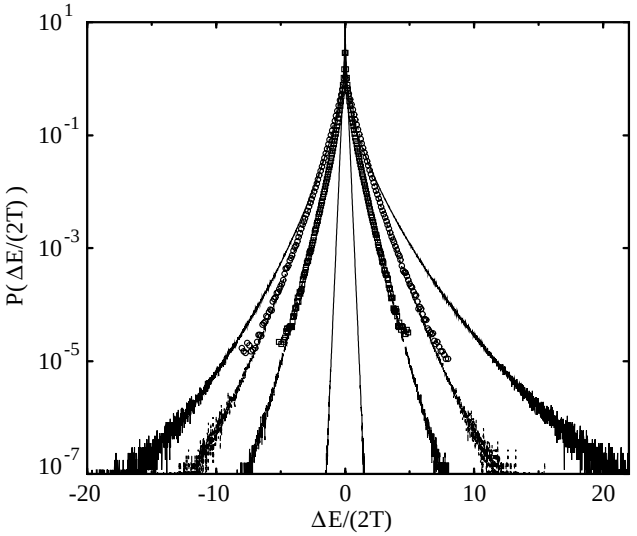

Fig. 3. MD (symbols) and DSMC (lines) simulations of the random α model. MD curves with packing fraction 10%. The various curves correspond to various $\rho(\alpha)$: from top to bottom (on the right), flat $\rho(\alpha)$ (DSMC), bimodal $\tilde{\rho}(\alpha^2) = \frac{1}{2}(\delta(\alpha^2 - 1/2) + \delta(\alpha^2 - 3/2))$ (DSMC and MD), uniform $\alpha^2 \in [0.5; 1.5]$ (DSMC and MD), and bimodal $\rho(\alpha) = \frac{1}{2}(\delta(\alpha - 1.04) + \delta(\alpha - 0.958332))$ (DSMC).

Moreover, in the case $\overline{\alpha^2} = 1$, expression (16) reduces to

$$a_2 = 16\frac{\overline{\alpha^4} - 1}{16d - 1 + 16(d-1)\overline{\alpha} - 15\overline{\alpha^4}}\,. \qquad (18)$$

The values of a_2 corresponding to the various distributions of normal restitutions shown in Figure 2, are given in Appendix A.

An important consequence of equation (16) is that the fourth cumulant depends only on $\overline{\alpha}$, $\overline{\alpha^2}$, and $\overline{\alpha^4}$: two different distributions $\rho(\alpha)$ having the same first, second and fourth moments should then yield very similar velocity distributions. This will be checked numerically in the next section and can be considered as a test for the consistency of the linear order approximation in a_2 underlying the analytical computation.

The question of the high-energy tail, which was addressed in [12,17] by neglecting the gain term in the collision integral $\tilde{I}$, turns out to be more problematic. Whenever α is allowed to take values exceeding 1, the gain term can no longer be discarded and we could not obtain analytical predictions. We shall therefore resort to a numerical resolution of the Boltzmann equation and to Molecular Dynamics simulations to analyze the high-velocity statistics. It can, however, be shown that the velocity distribution is Gaussian in the elastic case only (*i.e.* for $\rho(\alpha) = \delta(\alpha - 1)$, see Appendix B).

4.2 Numerics

We have simulated the IHS model with random restitution coefficient in two dimensions for various distributions $\rho(\alpha)$, both with DSMC and MD methods. The DSMC simulations were performed with $3{\cdot}10^5$ particles, the MD ones with up to 50000 particles, and packing fractions from 10% to 40%. The restitution coefficient α were drawn from distributions of various types: bimodal or trimodal distributions, flat distributions, flat distributions of α^2, Gaussian distributions of α^2 (with a cutoff in zero to ensure that $\alpha^2 \geq 0$). The distributions are shown in Figure 2: no large values of α or pathological distributions will be used.

The stationarity of the kinetic energy (following from $\overline{\alpha^2} = 1$) is controlled during the simulation, and allows to obtain in a single run the velocity distribution with a precision of typically 7 to 8 orders of magnitude. We first show in Figure 3 the histogram of the energy transfers during the collisions, corresponding to various $\rho(\alpha)$, for both DSMC and MD simulations; the similarity with the results of the 3-dimensional simulations (Fig. 1) allows to validate the model as far as energy transfer is concerned (the precise form of the histogram depends on the probability distributions $\rho(\alpha)$, but the qualitative features are those displayed by the projected 3D system considered in Sect. 3).

Figure 4 shows the velocity distributions for a flat $\tilde{\rho}(\alpha^2)$ between 0 and 2, for DSMC and MD simulations. The agreement between both sets of data is remarkable, and was also checked for other choices of $\rho(\alpha)$. Moreover, the curves obtained in MD simulations with small or large packing fractions (up to 40%) are indistinguishable (not shown). The inset shows that the distribution of impact parameters in Molecular Dynamics simulations is flat, which is a hint that no violation of molecular chaos is observed and an indication that the factorization of the

Table 1. Bimodal 1: $\frac{1}{2}(\delta(\alpha-\sqrt{1/2})+\delta(\alpha-\sqrt{3/2})$; bimodal 2: $\frac{1}{2}(\delta(\alpha-1.04)+\delta(\alpha-0.958332)$; flat α: $\alpha\in[0.457427;1.457427]$ trimodal: $\rho(\alpha)=\frac{b}{2}(\delta(\alpha-\sqrt{1+\gamma})+\delta(\alpha-\sqrt{1-\gamma}))+(1-b)\delta(\alpha-1)$; trimodal 1: $\gamma\approx 0.835254, b\approx 0.47779$; trimodal 2: $\gamma\approx 0.39058, b\approx 0.546248$; Gaussian: $\tilde{\rho}(\alpha^2)\propto\Theta(\alpha^2)\exp(-(\alpha^2-1)^2/(2s^2))$.

$\rho(\alpha)$	$\overline{\alpha}$	$\overline{\alpha^4}$	Theoretical a_2	Measured a_2
Bimodal 1	0.966	5/4	0.144	0.13
Bimodal 2	0.999	1.00666	$3.3\cdot10^{-3}$	$3.3\cdot10^{-3}$
Flat α	0.957	1.31111	0.187	0.162
Flat $\alpha^2\in[0;2]$	0.943	4/3	0.2	0.178
Trimodal 1	0.943	4/3	0.2	0.178
Flat $\alpha^2\in[0.5;1.5]$	0.989	1.0833	$4.4\cdot10^{-2}$	$4.2\cdot10^{-2}$
Trimodal 2	0.989	1.0833	$4.4\cdot10^{-2}$	$4.2\cdot10^{-2}$
Gaussian, $s=0.1$	0.986	1.09997	$5.3\cdot10^{-2}$	0.051
Gaussian, $s=0.2$	0.968	1.199	0.11	0.102

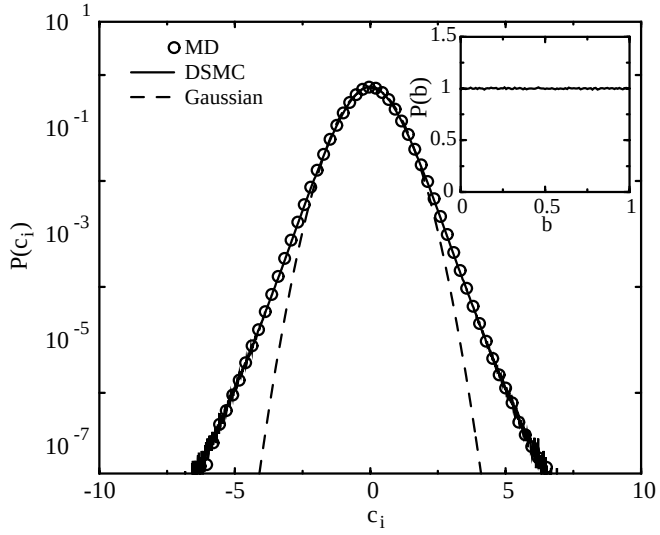

Fig. 4. Velocity distributions for the random α model, for MD (circles) and DSMC (solid line) simulations with, respectively, 50000 and 300000 particles, with the same $\rho(\alpha)$ (flat $\tilde{\rho}(\alpha^2)$ between 0 and 2). The agreement between both sets of data is striking. Large deviations from the Maxwellian (dashed line) are observed. The inset is the distribution of impact parameters for the MD simulations, showing no violation of molecular chaos.

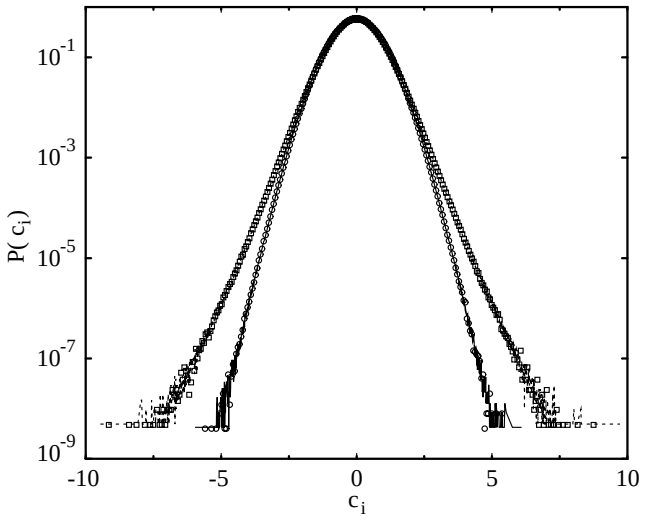

Fig. 5. Velocity distribution functions for DSMC simulations of the random α model, for two sets of two distributions having the same values of $\overline{\alpha}$ and $\overline{\alpha^4}$: Trimodal $\rho(\alpha)=\frac{b}{2}(\delta(\alpha-\sqrt{1+\gamma})+\delta(\alpha-\sqrt{1-\gamma}))+(1-b)\delta(\alpha-1)$ with $(b\approx 0.546248,\gamma\approx 0.390584)$ (solid line) *versus* a flat distribution for $\alpha^2\in[0.5;1.5]$ (circles), and another trimodal distribution with $(b\approx 0.47779,\gamma\approx 0.835254)$ (dotted line) *versus* another flat distribution for $\alpha^2\in[0:2]$ (squares). The agreement over 8 orders of magnitude shows that the a_2 approximation yields reliable predictions.

2-particle correlation function resulting in equation (3) holds. The super-imposition of MD (where *a priori* inhomogeneities and/or violations of molecular chaos could appear), and DSMC results is in contrast with the phenomenology at constant α [31] or with randomly driven IHS [32], and is probably due to an efficient randomization of the velocities with the collision rule of the present model. For a constant dissipative restitution parameter, colliding particles emerge with more parallel velocities than in the elastic case $\alpha=1$. When they recollide, their velocities are still more parallel. Here, this mechanism for the creation of velocity correlations violating molecular chaos seems removed by the possibility of having $\alpha>1$. This validates the theoretical approach based on the Boltzmann equation.

The remainder of this article is devoted to the deviations from Gaussianity that can be seen in Figure 4. To this aim, we shall use DSMC simulations that allow to obtain precise velocity distributions for a larger range of velocities than the MD method. However, as stated above, we always observed an excellent agreement between DSMC and MD velocity statistics, up to the resolution of MD.

The theoretical (from Eq. (16)) and measured (from the fourth moment of the velocity distribution) values of a_2 are given in Table 1. For small a_2 the measured and theoretical values agree perfectly, while for larger a_2 the agreement is worse, probably due to the neglect of quadratic a_2^2 and higher-order terms in the derivation of the theoretical formula. In fact the disagreement is at most

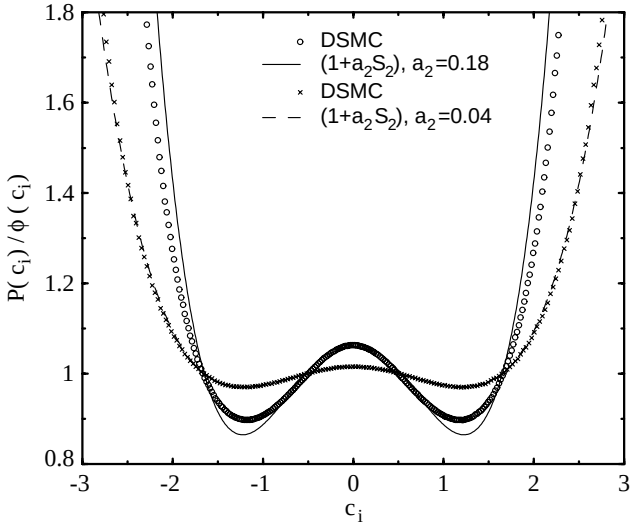

Fig. 6. Comparison of the ratios $\tilde{f}/\Phi$, measured in DSMC simulations (symbols), *versus* the theoretical predictions of the Sonine approximation $1 + a_2 S_2$ (lines), for two flat distributions of α^2: $\alpha^2 \in [0, 2]$ (circles) yields a relatively large fourth cumulant ($a_2 \approx 0.18$) and the agreement is satisfactory at small velocities only, while the measured and theoretical curves are indistinguishable for $\alpha^2 \in [0.5; 1.5]$ (crosses), for which $a_2 \approx 0.04$ is small.

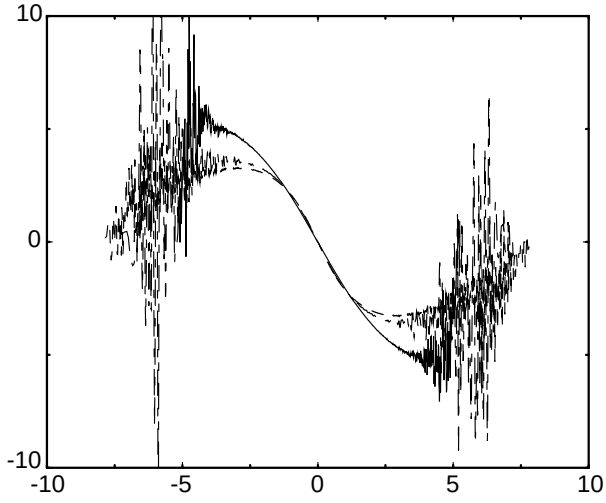

Fig. 7. Derivative $\mathrm{d} \ln \tilde{f}/\mathrm{d}c$ *versus* c for various $\rho(\alpha)$: from top to bottom on the right, flat $\tilde{\rho}(\alpha^2)$ with $\alpha^2 \in [0; 2]$, bimodal distribution $\tilde{\rho}(\alpha^2) = \frac{1}{2}[\delta(\alpha^2 - 1/2) + \delta(\alpha^2 - 3/2)]$, and flat $\tilde{\rho}(\alpha^2)$ in $[0.5, 1.5]$.

of 10% when $|a_2| > 0.1$, comparably to the results for constant α. As predicted, the same value of the fourth cumulant a_2 is associated with distributions having the same first, second and fourth moments (see Eq. (18)). Moreover, Figure 5 shows strong numerical evidence that, *in this case*, the whole distributions of velocities are indistinguishable, *i.e.* not only a_2 but the complete statistics (including large velocities) depend only on the first moments of $\rho(\alpha)$. Of course, for other $\rho(\alpha)$, this property may not be true any more.

In Figure 6, we show the comparison between the normalized velocity distribution for two distributions of restitution coefficients, together with the Sonine prediction $1 + a_2 S_2$. In the case of small a_2, the agreement is striking: the Sonine expansion is supposed to be valid for small values of c, while we see in Figure 6 an agreement up to relatively large c. For larger a_2, the global shape corresponds to the prediction, but the quantitative agreement is lost. This is quite expected since, when a_2 is not very small, higher-order terms in the Sonine expansion become relevant.

We now turn to the study of the large velocity tails. A first indication is given by the plot of the derivative of $\ln \tilde{f}(c)$, which is linear for a Gaussian, and constant for an exponential law. An $\exp(-Ac^B)$ tail, on the other hand, leads to a c^{B-1} behaviour. We see in Figure 7 that the non-Gaussianity is indeed revealed by this criterion, but that the numerical noise hinders any clear conclusion on the value of B. Since our velocity statistics are smooth over 8 orders of magnitude, this approach is unable to determine the values of B, even if $f(v)$ behaves asymptotically as a stretched exponential.

Figure 8, on the other hand, shows three fits, for three distributions of restitution coefficients. These fits are of the form $\exp(-Ac^B)$, and we obtain a wide range of possible values for B [1]: from 0.8 to 2, with fits accurate over 6 orders in magnitude. In particular, a convenient choice of $\rho(\alpha)$ is compatible with $B = 1.6$, which has been found in some experiments [4,5] (close to $B = 3/2$ obtained in [17] for randomly driven IHS fluids). The corresponding $\rho(\alpha)$ (trimodal $\rho(\alpha) = \frac{b}{2}(\delta(\alpha - \sqrt{1+\gamma}) + \delta(\alpha - \sqrt{1-\gamma})) + (1-b)\delta(\alpha - 1)$ with $(b \approx 0.546248, \gamma \approx 0.390584)$, or equivalently flat $\alpha^2 \in [0.5, 1.5]$), is not very broad and does not imply the use of particularly large values of α. Other choices of $\rho(\alpha)$ can also lead to an exponential tail ($B = 1$), similarly to the case of the homogeneous cooling state (constant $\alpha < 1$, with no heating), or even to larger distributions with $B < 1$.

5 One-dimensional case

For completeness, we briefly report the results obtained for the one-dimensional version of the random α model; it should correspond to a projection in one dimension of a two-dimensional system, with energy injection along the projection direction.

The study of the projected model defined in Section 3 (injection of energy by randomly drawing the y-component of the velocity after each collision) yields similar results as those obtained in the case of a three-dimensional system projected in 2D.

The random α model, however, displays a certain number of pathologies: for $d = 1$ and $\overline{\alpha^2} = 1$, we obtain analytically $a_2 = -16/15$ from equation (18). This large value, independent of $\rho(\alpha)$ (*i.e.* non-perturbative), indicates that

[1] As stated above, for the situations investigated, the value of B seems to depend on the first moments of $\rho(\alpha)$ only.

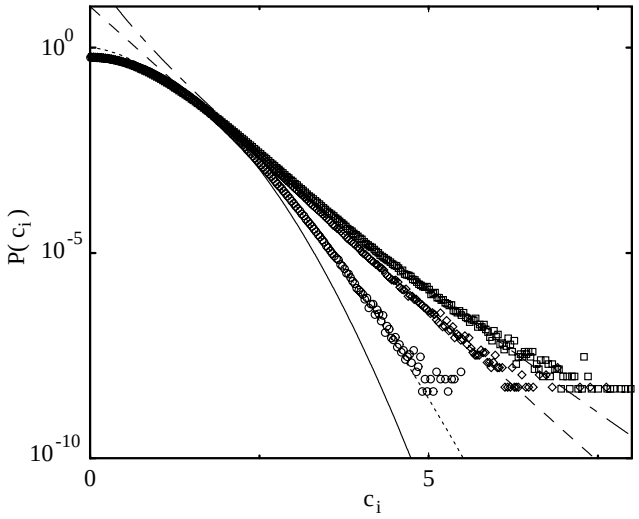

Fig. 8. Velocity distributions for the same $\rho(\alpha)$ as in Figure 7 (circles: flat $\tilde{\rho}(\alpha^2)$ in $[0.5, 1.5]$; diamonds: bimodal $\alpha^2 = 1/2$ or $3/2$; squares: flat $\tilde{\rho}(\alpha^2)$ in $[0; 2]$), obtained from DSMC simulations, together with the Maxwellian Φ (solid line) and fits to $K\exp(-Ac^B)$ (dotted line: $\exp(-1.5c^{1.6})$; dashed line: $10\exp(-3.4c)$; dot-dashed line: $100\exp(-5c^{0.8})$). The fits are accurate over 6 orders of magnitude and values of B consistent with the experimental data ($B \approx 1.6$) can be obtained for a convenient choice of $\rho(\alpha)$.

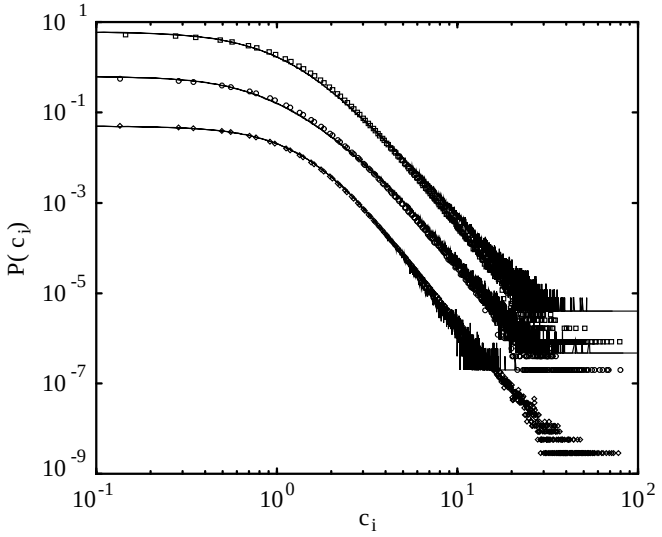

Fig. 9. Velocity distributions for the one-dimensional case, for various $\rho(\alpha)$: flat ρ (middle), flat $\tilde{\rho}$ ($\alpha^2 \in [0.5; 1.5]$) (top), and bimodal $\rho(\alpha) = \frac{1}{2}(\delta(\alpha-1.04)+\delta(\alpha-0.958332))$ (bottom). Data for DSMC (symbols) and MD (lines) simulations are shown. Some distributions have been shifted for clarity.

the Sonine expansion is not valid. In fact, numerical investigations (both MD and DSMC) show that the velocity distributions $f(v)$ have power law tails (see Fig. 9). This behaviour differs significantly from a Gaussian and explains the failure of the Sonine approximation.

6 Summary and conclusions

We have introduced the idea of a random restitution coefficient in the IHS model to describe a vertically vibrated layer of granular material. Since energy is injected only along the vertical axis, and transferred through collisions in the perpendicular directions, our approach accounts for the fact (as shown in Sect. 3) that the projection in 2 dimensions of a 3-dimensional collision can correspond to a gain in the two-dimensional energy, and therefore to an effective restitution coefficient α larger than 1, even if the genuine α necessarily corresponds to a dissipative collision. The model is consequently studied in 2 dimensions, with a probability distribution $\rho(\alpha)$ for the restitution coefficient. We have analyzed the velocity distributions, and, in particular, the deviation from the Maxwellian, using the Sonine expansion technique. Following [17] we obtained analytically the expression of the fourth cumulant a_2, which has been tested against Molecular Dynamics (MD) and Monte Carlo Direct Simulations (DSMC). It turns out that the theoretical predictions for a_2 are quite accurate, with a slight overestimation for a_2 that probably corresponds to the approximations made during the calculation (non-linear terms $\mathcal{O}(a_2^2)$ and higher-order Sonine polynomials neglected); in particular, a_2 depends only on the first moments of $\rho(\alpha)$; numerically, *the whole velocity distribution* has the same property with a very high precision, at least for the $\rho(\alpha)$ studied here (we do not exclude that this behaviour could be violated by other kinds of distributions). Moreover, the comparison between numerical data and the second-order Sonine expansion shows a remarkable agreement for small values of a_2. The high-energy tails, studied with DSMC simulations, can be fitted by functions of the form $\exp(-Ac^B)$, with $B < 2$ depending on $\rho(\alpha)$. It would certainly be interesting to have theoretical predictions concerning B; it seems, for example, that the high-energy tail is always overpopulated with respect to the Maxwellian, while a particular choice of heating can also yield an under-population, as shown in [20]. Note that once a functional form has been chosen for $\rho(\alpha)$, very different tails can be observed depending on the range of variation for α (compare the circles and squares in Fig. 8). This feature might question the relevance of the exponent B as an intrinsic quantity for granular gases in steady states.

An interesting issue concerns the fact that no violation of molecular chaos has been observed: MD and DSMC results are in remarkable agreement (even with a packing fraction as high as 40% in MD). This is in contrast with the situation of free cooling [31] but also with MD results on heated inelastic hard spheres [32]. The microscopic precollisional velocity correlations driven by the standard inelastic collision rule with a constant restitution coefficient [33] seem significantly reduced within the present random α model. A thorough investigation of short-scale velocity correlations would require the computation of various precollisional averages involving moments of the relative velocities, and has not been performed. Our results, however, suggest that the dynamical correlations inducing

recollisions [34] and responsible for the violation of molecular chaos may not be a generic feature of driven granular gases exhibiting a non-equilibrium stationary state.

More refined models could introduce correlations between the effective restitution coefficient and the relative velocities of colliding pairs. This feature, neglected here, seems difficult to quantify from first principles, but might affect the high-energy tail or induce precollisional velocity correlations. It would, however, be very interesting to be able to link a realistic energy injection mechanism with a precise distribution of restitution coefficients.

Finally, a hydrodynamic study of the present random α model, in which the conservation of the energy is valid on average only, is left for future investigations.

Appendix A. Fourth cumulant of the velocity distribution

In this appendix, we consider particular distributions $\rho(\alpha)$ (with $\overline{\alpha^2}=1$), and give the corresponding formulae for a_2.

- Trimodal $\rho(\alpha)=\frac{b}{2}[\delta(\alpha-\sqrt{1+\gamma})+\delta(\alpha-\sqrt{1-\gamma})]+(1-b)\delta(\alpha-1)$:

$$a_2=\frac{16b\gamma^2}{8b(\sqrt{1+\gamma}+\sqrt{1-\gamma})+32-16b-15b\gamma^2}\,. \quad \text{(A.1)}$$

- Bimodal $\rho(\alpha)=\frac{1}{2}(\delta(\alpha-\sqrt{1+\gamma})+\delta(\alpha-\sqrt{1-\gamma}))$ (particular case of the trimodal distribution, with $b=1$):

$$a_2=\frac{16\gamma^2}{16-15\gamma^2+8(\sqrt{1+\gamma}+\sqrt{1-\gamma})}\,. \quad \text{(A.2)}$$

  Example: for $\gamma=0.5$, $a_2\approx 0.1444$.
- Flat distribution for α^2, between $1-\gamma$ and $1+\gamma$:

$$a_2=\frac{16\gamma^3}{16\left((1+\gamma)^{3/2}-(1-\gamma)^{3/2}\right)+48\gamma-15\gamma^3}\,. \quad \text{(A.3)}$$

  Example: for $\gamma=0.5$, $a_2\approx 0.0436$; for $\gamma=1$, $a_2\approx 0.2045$.
- Flat distribution for α, between γ and $1+\gamma$: $\overline{\alpha^2}=1$ imposes $\gamma=(\sqrt{11/3}-1)/2$, and yields $a_2\approx 0.1868$.

Appendix B. Gaussian iff $\rho=\delta(\alpha-1)$

We show in this appendix that only the trivial elastic distribution $\rho(\alpha)=\delta(\alpha-1)$ can lead to Gaussian velocity statistics.

Since we assume $\overline{\alpha^2}=1$, $\mu_2=0$ (see Sect. 4.1). Therefore, equation (6) reduces to

$$\int \mathrm{d}\alpha\rho(\alpha)\tilde{I}(\tilde{f},\tilde{f})=0\,. \quad \text{(B.1)}$$

Let us assume that $\tilde{f}(c)$ is Gaussian. The equations for $\mathbf{v}_1^{**}$ and $\mathbf{v}_2^{**}$ lead to

$$\tilde{f}(c_1^{**})\tilde{f}(c_2^{**})=\tilde{f}(c_1)\tilde{f}(c_2)\exp\left(-\frac{\alpha^{-2}-1}{2}(\mathbf{c}_{12}\cdot\hat{\boldsymbol{\sigma}})^2\right). \quad \text{(B.2)}$$

Equation (B.1) is then recast, by carrying out the integration over α for the term $\tilde{f}(c_1)\tilde{f}(c_2)$, and simplifying by $\tilde{f}(c_1)$, into

$$\gamma_d I_d\int \mathrm{d}\mathbf{c}_2 c_{12}\tilde{f}(c_2)=\int \mathrm{d}\alpha\frac{\rho(\alpha)}{\alpha^2}\int \mathrm{d}\mathbf{c}_2 c_{12}\tilde{f}(c_2)J_d\,, \quad \text{(B.3)}$$

where

$$\begin{aligned}\gamma_d I_d&=\gamma_d\int_{-\pi/2}^{\pi/2}\mathrm{d}\theta\sin^{d-2}\theta\cos\theta\,,\\ J_d&=\int'\mathrm{d}\hat{\boldsymbol{\sigma}}\cos\theta\exp\left(-\frac{\alpha^{-2}-1}{2}(c_{12}\cos\theta)^2\right),\\ &=\gamma_d\int_{-\pi/2}^{\pi/2}\mathrm{d}\theta\sin^{d-2}\theta\cos\theta\\ &\quad\times\exp\left(-\frac{\alpha^{-2}-1}{2}(c_{12}\cos\theta)^2\right). \quad \text{(B.4)}\end{aligned}$$

θ is the angle between $\hat{\boldsymbol{\sigma}}$ and $\mathbf{c}_{12}$, and γ_d is a geometrical factor corresponding to the integration over the remaining angles. By expanding the exponential, we thus obtain the relation *valid for any* $\mathbf{c}_1$:

$$\begin{aligned}0&=I_d\int \mathrm{d}\mathbf{c}_2 c_{12}\tilde{f}(c_2)-\int \mathrm{d}\alpha\frac{\rho(\alpha)}{\alpha^2}\\ &\quad\times\int \mathrm{d}\mathbf{c}_2\tilde{f}(c_2)\sum_{p=0}^{\infty}\left(\frac{1-\alpha^{-2}}{2}\right)^p c_{12}^{2p+1}\\ &\quad\times\int_{-\pi/2}^{\pi/2}\mathrm{d}\theta\sin^{d-2}\theta\cos^{2p+1}\theta\,. \quad \text{(B.5)}\end{aligned}$$

Since this is valid for any $\mathbf{c}_1$, each term of the expansion in powers of c_{12} must be zero. For $p=0$ we obtain

$$\overline{\alpha^{-2}}=1\,, \quad \text{(B.6)}$$

and for $p\geq 1$

$$\overline{\alpha^{-2}(1-\alpha^{-2})^p}=0. \quad \text{(B.7)}$$

A straightforward recurrence yields $\overline{\alpha^{-2p}}=1$ for any $p\geq 0$, and thus

$$\rho(\alpha)=\delta(\alpha-1)\,. \quad \text{(B.8)}$$

References

1. E. Clement, J. Rajchenbach, Europhys. Lett. **16**, 133 (1991).
2. S. Warr, G.T.H Jacques, J.M. Huntley, Powder Tech. **81**, 41 (1994); S. Warr, J.M. Huntley, G.T.H Jacques, Phys. Rev. E **52**, 5583 (1995).
3. J.S. Olafsen, J.S. Urbach, Phys. Rev. Lett. **81**, 4369 (1998); Phys. Rev. E **60**, R2468 (1999).
4. W. Losert, D.G.W. Cooper, J. Delour, A. Kudrolli, J.P. Gollub, Chaos **9**, 682 (1999) and cond-mat/9901203.
5. F. Rouyer, N. Menon, Phys. Rev. Lett. **85**, 3676 (2000).
6. A. Kudrolli, J. Henry, Phys. Rev. E **62**, R1489 (2000).
7. S. Luding, H.J. Herrmann, Chaos **9**, 673 (1999).
8. T.P.C. van Noije, M.H. Ernst, Phys. Rev. E **61**, 1765 (2000).
9. I. Goldhirsch, G. Zanetti, Phys. Rev. Lett. **70**, 1619 (1993).
10. S. McNamara, W.R. Young, Phys. Rev. E **53**, 5089 (1996).
11. J.J. Brey, M.J. Ruiz-Montero, D. Cubero, Phys. Rev. E **54**, 3664 (1996).
12. S.E. Esipov, T. Pöschel, J. Stat. Phys. **86**, 1385 (1997).
13. N.V. Brilliantov, T. Pöschel, Phys. Rev. E **61**, 2809 (2000); **61**, 5573 (2000).
14. M. Huthmann, J.A.G. Orza, R. Brito, cond-mat/0004079.
15. D.R. Williams, F.C. MacKintosh, Phys. Rev. E **54**, R9 (1996).
16. A. Puglisi, V. Loreto, U. Marini Bettolo Marconi, A. Vulpiani, Phys. Rev. E **59**, 5582 (1999).
17. T.P.C. van Noije, M.H. Ernst, Granular Matter **1**, 57 (1998).
18. T.P.C. van Noije, M.H. Ernst, E. Trizac, I. Pagonabarraga, Phys. Rev. E **59**, 4326 (1999).
19. R. Cafiero, S. Luding, H.J. Herrmann, Phys. Rev. Lett. **84**, 6014 (2000).
20. J.M. Montanero, A. Santos, Granular Matter **2**, 53 (2000).
21. X. Nie, E. Ben-Naim, S.Y. Chen, Europhys. Lett. **51**, 679 (2000).
22. T. Aspelmeier, A. Zippelius, Physica A **282**, 450 (2000).
23. P. Résibois, M. de Leener, *Classical Kinetic Theory of Fluids* (John Wiley and Sons, 1977).
24. A. Goldshtein, M. Shapiro, J. Fluid Mech. **282**, 75 (1995).
25. L. Landau, E. Lifshitz, *Physical Kinetics* (Pergamon Press, 1981).
26. G. Bird, *Molecular Gas Dynamics* (Oxford University Press, New York, 1976) and *Molecular Gas Dynamics and the Direct Simulation of Gas Flows* (Clarendon Press, Oxford, 1994).
27. J.J. Brey, D. Cubero, M.J. Ruiz-Montero, Phys. Rev. E **59**, 1256 (1999).
28. See, *e.g.*, H.J. Herrmann, in *Disorder and Granular Media*, edited by D. Bideau, A. Hansen (Elsevier Science Publisher, 1993).
29. M.P. Allen, D.J. Tildesley *Computer Simulations of Liquids* (Clarendon Press, Oxford, 1987).
30. K. Helal, T. Biben, J.P. Hansen, Physica A **240**, 361 (1997).
31. S. Luding, *GAMM '99 Proceedings*, ZAMM **80**, 9 (2000).
32. I. Pagonabarraga, E. Trizac, T.P.C. van Noije, M.H. Ernst, in preparation.
33. R. Soto, M. Mareschal, Phys. Rev. E **63**, 041303 (2001).
34. J.R. Dorfman, H. van Beijeren, *The Kinetic Theory of Gases*, in *Statistical Mechanics, Part B: Time-Dependent Processes*, edited by B.J. Berne (Plenum Press, New York, 1977) Chapt. 3.